

**REPORT DOCUMENTATION PAGE**

*Form Approved*  
OMB No. 0704-0188

The public reporting burden for this collection of information is estimated to average 1 hour per response, including the time for reviewing instructions, searching existing data sources, gathering and maintaining the data needed, and completing and reviewing the collection of information. Send comments regarding this burden estimate or any other aspect of this collection of information, including suggestions for reducing the burden, to Department of Defense, Washington Headquarters Services, Directorate for Information Operations and Reports (0704-0188), 1215 Jefferson Davis Highway, Suite 1204, Arlington, VA 22202-4302. Respondents should be aware that notwithstanding any other provision of law, no person shall be subject to any penalty for failing to comply with a collection of information if it does not display a currently valid OMB control number.

**PLEASE DO NOT RETURN YOUR FORM TO THE ABOVE ADDRESS.**

1. REPORT DATE (DD-MM-YYYY) 04-04-2007		2. REPORT TYPE Interim Report		3. DATES COVERED (From - To) August 2006-December 2006	
4. TITLE AND SUBTITLE  Strain Mapping in Nanostructured Coatings by Synchrotron Radiation				5a. CONTRACT NUMBER	
				5b. GRANT NUMBER N00014-06-1-0880	
				5c. PROGRAM ELEMENT NUMBER	
6. AUTHOR(S)  Thomas Tsakalagos (PI), Mark Croft (Co-PI), Dr. Rajendra Sadangi and Dr. Vijay Shukla				5d. PROJECT NUMBER 07PR02131-00	
				5e. TASK NUMBER	
				5f. WORK UNIT NUMBER	
7. PERFORMING ORGANIZATION NAME(S) AND ADDRESS(ES) Rutgers, The State University of New Jersey New Brunswick, NJ 08901				8. PERFORMING ORGANIZATION REPORT NUMBER	
9. SPONSORING/MONITORING AGENCY NAME(S) AND ADDRESS(ES) Office of Naval Research 495 Summer Street Suite 627 Boston, MA 02210-2109				10. SPONSOR/MONITOR'S ACRONYM(S) ONR	
				11. SPONSOR/MONITOR'S REPORT NUMBER(S)	
12. DISTRIBUTION/AVAILABILITY STATEMENT "Approved for Public Release; Distribution is unlimited".					
13. SUPPLEMENTARY NOTES					
<h1>20070907330</h1>					
14. ABSTRACT  We report an Energy Dispersive X-ray Diffraction (EDXRD) method to determine the local strain field in a plasma sprayed Alumina-13% Titania ceramic coating. The measurements were carried out using high energy photons (100-300 KeV) on the X17B1 beamline at Brookhaven National Laboratory. The phase distribution of phases in the coatings produced from plasma spraying of micron size and agglomerated nanosize powder is described.					
15. SUBJECT TERMS  EDXRD, Phase Mapping, Nanostructured Coatings					
16. SECURITY CLASSIFICATION OF:			17. LIMITATION OF ABSTRACT	18. NUMBER OF PAGES 11	19a. NAME OF RESPONSIBLE PERSON
a. REPORT	b. ABSTRACT	c. THIS PAGE			19b. TELEPHONE NUMBER (Include area code)

<b>Contract Number</b>	N00014-06-1-0880
<b>Title of Research</b>	Strain Mapping in Nanostructured Coatings by Synchrotron Radiation
<b>Report Period</b>	August 2006 – December 2006
<b>Principal Investigators</b>	Thomas Tsakalakos (PI), Mark Croft (Co-PI)
<b>Researchers</b>	Dr. Rajendra Sadangi and Dr. Vijay Shukla
<b>Organization</b>	Materials Science and Engineering Dept. and Physics Dept. at Rutgers university

## 1. Objectives

The long term objectives of this project are:

- To measure strain and phase distribution profiles in coatings in order to understand differences in their performance and durability
- To determine the grain size dependence of internal residual stresses in coatings.
- To characterize the buildup of such stresses during the formation of coatings used in the Navy.

## 2. Project Status

This report describes the work done on this project during the period August 2006 – December 2006. The project is in the initial stages of a two year research program focused on alumina-titania coating.

To understand the influence of coating thickness and substrate material a set of coatings were procured and experiments performed during October 2006. Analysis of these experiments has found that the choice of 1020 steel as a substrate material was not appropriate and new samples using 4142 steel will be used in future experiments. These preliminary experiments have been useful in characterizing the problems of data collection, on coatings. We expect that this preliminary work will help in the project in the future.

## 3. Coating Samples

Plasma-sprayed ceramic coatings are used to protect metallic structural components from corrosion, wear, and erosion, and to provide lubrication and thermal insulation. In particular, Navy has been using coatings made of  $\text{Al}_2\text{O}_3$  containing 13 wt%  $\text{TiO}_2$ . In the plasma-spray coating deposition process, feed powder particles are injected into a plasma jet, causing them to melt into droplets that are propelled towards the substrate. Solidification of the droplet stream onto the substrate as “splats” results in the buildup of the coating [ 1], typically 100–300  $\mu\text{m}$  thick.

The coatings produced by two distinct types of feed powders will be compared in this research project. The first is a conventional (or micro) feed powder with a mixture of  $\text{Al}_2\text{O}_3$  and  $\text{TiO}_2$  powders. The conventional feed powder used is a commercial available powder Metco-130, from Sulzer Metco, Westbury, NY. The powder particles are angular in shape (30–50  $\mu\text{m}$  diameter), and they consist of fused and crushed  $\text{Al}_2\text{O}_3$  clad with a  $\text{TiO}_2$  layer. To deposit coatings, these powders are processed using a high enthalpy plasma, which ensures near complete melting of the powder particles. Such conventional feed powders and the resulting coatings will be referred to below with the “conventional-“ and/or “micro-“ prefix.

The second type of coating is a deposited using a nano-scale starting powder, 2613PA, manufactured by Inframat. This nano-feed powder is crushed, spray-dried and plasma-densified. Its alumina grain size, measured by transmission electron microscopy, ranges from a few to 150 nm, with an average of 40 nm. Chemical homogeneity in the nanosized feed powder, is obtained by using a two-step processing method. In the first step, nanocrystalline  $\text{Al}_2\text{O}_3$  and  $\text{TiO}_2$  powders, plus small amounts of other additives (e.g. ceria and zirconia), are mixed in appropriate proportions and spray-dried to obtain agglomerates of size 30–50  $\mu\text{m}$ . In the second step, these agglomerates are injected into the plasma torch and the partially or fully molten ceramic droplets are collected in water (plasma densification). Using these powder particles as the feedstock, and by controlling the plasma-spray parameters, the microstructure of such “nano-“coatings can be controlled. In the formation of these coatings, a lower enthalpy plasma can be used. The parameters can be used to generate a coating with either fully molten, partially molten or un-molten, powders resulting in a complex coating microstructure [2,3].

The durability of nano-coating of  $\text{Al}_2\text{O}_3$ -13wt% $\text{TiO}_2$  has been observed to be superior to that of micro-coatings of the same base material. This observation motivates the present program in which we wish to compare the phases and strains present in  $\text{Al}_2\text{O}_3$ -13wt% $\text{TiO}_2$  coatings made from starting micron size (Metco 130) to those in coatings prepared from nanosized powders (Inframat 2613). In addition we wish to compare the phases and strains as a function of coating thickness in both micro- and nano- coatings. Accordingly two substrate materials, 1020 steel (with a Ni bond coat) and titanium (with a Ti bond coat), were used as substrate materials on which varying thickness of micro- and nano- coatings were applied. Substrates with no coating and only grit blasting were also retained to serve as standards during the measurements. Table 1, summarizes the coating samples produced with 1020 steel and also the experiments performed till date. Table 2 is similar for the titanium substrate coating samples produced. All the samples were prepared by A&A company, which is a Navy approved thermal spray shop.

Starting Powder	Substrate	Coating thickness	Designation	Comment
Micron	1020 steel	None	S1	All experiments on steel substrates completed, but results are not conclusive. We plan to redo these coatings on small grain size 4142 steel.
		Grit blast only	S2	
		Grit blast and bond coat	S3	
		2 passes on S3	S4	
		Typical coating on S3	S5	
		Over-coating, on S3, before failure	S6	
		Over-coating, on S3, after failure	S7	
Nanosize	1020 steel	2 passes on S3	S8	
		Typical coating on S3	S9	
		Over-coating, on S3, before failure	S10	
		Over-coating, on S3, after failure	S11	

Table 1. Coating samples produced using steel substrates. Whether experiments are performed or not is indicated in the comments column.

Starting Powder	Substrate	Coating thickness	Designation	Comment
Micron	Titanium	None	T1	Experiments complete
		Grit blast only	T2	
		Grit blast and bond coat	T3	Experiments pending
		2 passes on T3	T4	
		Typical coating on T3	T5	
		Over-coating, on T3, before failure	T6	Data discarded due to stepper motor control problems
		Over-coating, on T3, after failure	T7	
Nanosize	Titanium	2 passes on T3	T8	Experiments pending
		Typical coating on T3	T9	
		Over-coating, on T3, before failure	T10	
		Over-coating, on T3, after failure	T11	

Table 2. Coating samples produced using titanium substrates. Whether experiments are performed or not is indicated in the comments column.

## 4. Phase mapping Results

The service life-prolonging plasma sprayed ceramic coatings being studied in this project are complex. Moreover, the grit blasting pretreatment, varying substrate metals and varying intervening on coating materials increase the complexity. A careful study of the phases occurring in these substrate/bond-coat/ceramic-coating systems must be undertaken concurrently with the strain profiling measurements. Cross-sectioning of the x-ray diffraction patterns, at depth intervals as small as 20  $\mu\text{m}$ , of such substrate/bond-coat/ceramic-coating systems has been performed using synchrotron based EDXRD measurements at Brookhaven National Labs.

### 4.1 Phase mapping: micro-coating

In Figure 4.1-1 (top) such a diffraction cross-sectioning of the top  $\sim 300 \mu\text{m}$  of a micro-coated 1020 steel specimen is shown with the vertical axis on the plot being the depth along the  $x_3$  direction and the colors of the contour plot being scaled with red being high intensity and blue being low intensity. In Figure 4.1-1 (bottom) simulations of the diffraction patterns for the relevant phases is shown. Here it should be noted that while these simulations predict the nominal Bragg line positions for comparison to EDXRD, the diffraction peak amplitudes cannot be directly compared. Proper account of the strong absorption effects in our thick specimens and the energy dependence of the atomic scattering factors is *not* accounted for in the simulation.

Referring to Figure 4.1-1 the bcc-Fe steel Bragg line just above 100 keV marking the top of the substrate can be seen at the bottom of the contour plot. Here the Fe-Bragg lines below 100 keV are suppressed by the strong absorption in the 25 mm path length traversing the steel substrate. The Bragg lines of the fcc-Ni bond (compared to the simulation) coat layer can clearly be discerned above the steel. Finally, the Bragg lines in the coating are seen to be dominantly of the cubic defect spinel  $\gamma\text{-Al}_2\text{O}_3$  structure. Closer inspection of the data by other methods reveals small amounts of corundum  $\alpha\text{-Al}_2\text{O}_3$  structure, along with substantial amorphous components.

Figure 4.1-2 shows a similar contour plot on a depth scale traversing the entire specimen depth and a wider energy range. The full extent of the steel, bond coat, and ceramic coating can be seen in this figure.

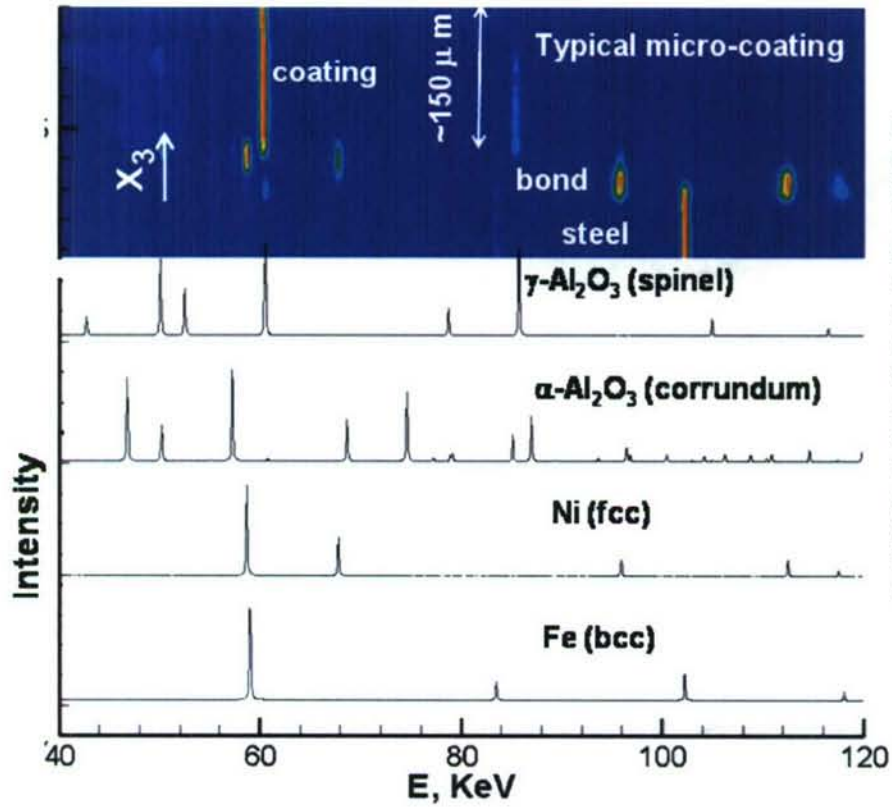


Figure 4.1-1 Synchrotron x-ray phase profiling for a micro-titanium alumina coating on a 1020 steel substrate. Bottom: a simulation of the diffraction spectrum, showing the positions of the Bragg lines of the steel substrate, Ni bonding coating, and the spinel and corundum phases of alumina. Top: A contour plot of the variations with depth ( $x_3$ ) in the Bragg line energy positions and intensities (in color with red being high intensity) within the  $\sim 300 \mu\text{m}$  of the coatings free surface.

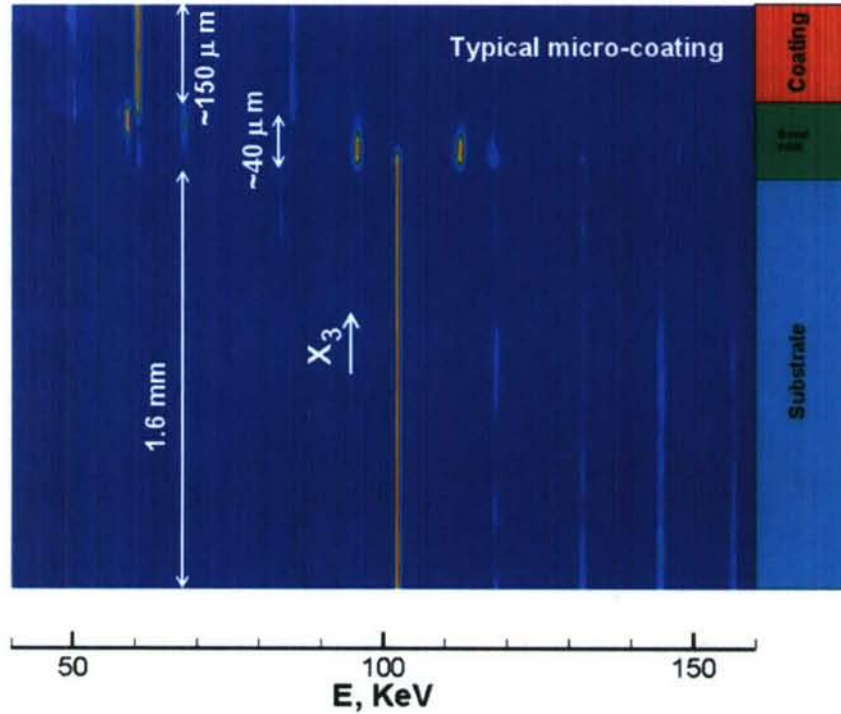


Figure 4.1-2 A view of the contour plot, from the figure above, spanning the entire coating, bond coating and substrate regions of the specimen.

## 4.2 Phase mapping: nano-coating

Proceeding in analogy to the section 4.1, immediately above, Figure 4.2-1 (top) shows a diffraction cross-sectioning of the top  $\sim 300 \mu\text{m}$  of a nano-coated 1020 steel specimen. Again comparison to the simulations, in Figure 4.2-1 (bottom), clearly reveals the bcc-Fe steel substrate region along with the the fcc-Ni bond coat layer. Also again the coating is seen to be dominantly of the cubic defect spinel  $\gamma\text{-Al}_2\text{O}_3$  structure. In the case of the nano coating however it appears that the minority corundum  $\alpha\text{-Al}_2\text{O}_3$  structure component makes a somewhat stronger contribution. Although this is clear in other data display methods the  $\alpha\text{-Al}_2\text{O}_3$  Bragg line near 73 keV is discernible. Moreover,  $\alpha\text{-Al}_2\text{O}_3$  Bragg lines flanking the strong  $\gamma\text{-Al}_2\text{O}_3$  Bragg line at  $\sim 83$  keV can also be observed under close inspection. Figure 4.2-2, illustrates the full extent of the steel, bond coat, and ceramic coating with a contour plot on a depth scale traversing the entire specimen and a wider energy range.

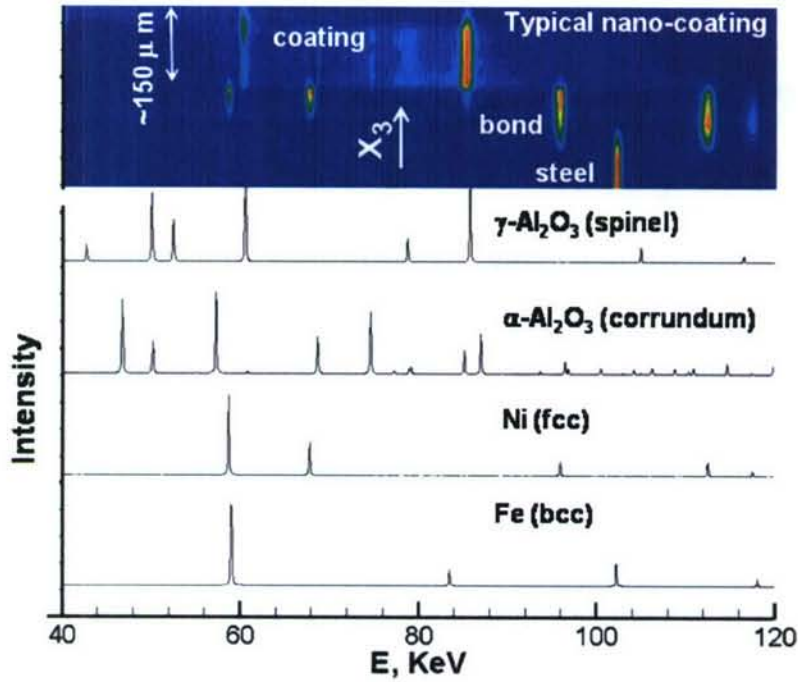


Figure 4.2-1 Synchrotron x-ray phase profiling for a nano-titanium alumina coating on a 1020 steel substrate. Bottom: a simulation of the diffraction spectrum, showing the positions of the Bragg lines of the steel substrate, Ni bonding coating, and the spinel and corundum phases of alumina. Top: A contour plot of the variations with depth ( $x_3$ ) in the Bragg line energy positions and intensities (in color with red being high intensity) within the  $\sim 300 \mu\text{m}$  of the coatings free surface.

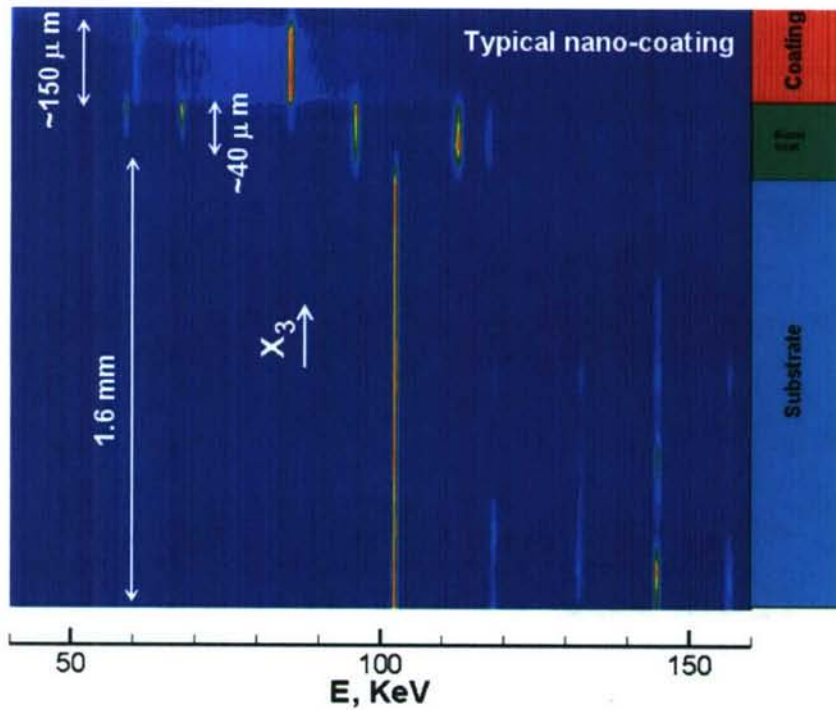


Figure 4.2-2 A view of the contour plot, from the figure above, spanning the entire coating, bond coat, and substrate regions of the specimen.

## 5. Conclusions

Analysis of the strain induced Bragg line shifts in the 1020 steel substrate material has substantial scatter due to local inter-granular strain (Type II residual stress). This suggests that this substrate material is not optimal for studying these substrate-coating stress interactions. We will change the substrate material to 4140 steel which has a finer grain size. The phase mapping results show that spinel  $\gamma$ -Al<sub>2</sub>O<sub>3</sub> Bragg lines are intense enough for EDXRD strain field profiling.

## 6. Appendix: Experimental Technique

In order to perform high spatial resolution strain mapping thin coatings on a thick substrate materials we utilize a highly collimated incident x-ray beam directed parallel to the coating surface (see Figure A1) [4-6]. Here the beam dimension perpendicular to the surface,  $d_i$ , is a down to  $\sim 20$   $\mu\text{m}$  to provide the necessary resolution through the coating and substrate interface. Here scattered beam collimation  $d_s$  is opened to 100-300  $\mu\text{m}$  to achieve higher count rates. The gauge volume thus to find (see Figure A1) is elongated parallel to the service direction but remain small  $\sim 20$   $\mu\text{m}$  in the surface normal direction.

A schematic of the x-ray scattering geometry with respect to the interatomic planes is shown in Figure A2, the energy ( $E$ ), wavelength ( $\lambda$ ) and wave number ( $k$ ) of the x-ray photons along with the incoming ( $\mathbf{k}_{in}$ ) outgoing ( $\mathbf{k}_{out}$ ) and scattering ( $\Delta\mathbf{k}_{in}$ ) wave vectors are indicated. Note the scattering wave vector is parallel to the unit vector in the  $i$ 'th direction ( $i=1,2,$  and  $3$  for  $x_1, x_2$  and  $x_3$ ) and perpendicular to the  $\{h,k,l\}$  interatomic planes. Note the strain component  $\varepsilon_{ii}$  is measured in this geometry.. The Bragg reflections, from the atomic planes (spaced at distances  $d_{hkl}$ ), are collected as a function of energy. The relation between the energy and a specific interatomic-plane spacing is [4-6]

$$E_{hkl} = \frac{6.199}{\sin \theta} \cdot \frac{1}{d_{hkl}} \quad (1)$$

Here, the fixed scattering angle is  $2\theta$  ( $2\theta \sim 3^\circ$ - $15^\circ$ ),  $\{hkl\}$  are the Miller indices identifying the crystalline planes,  $E_{hkl}$  the energy of an  $\{hkl\}$  reflection and the units for this expression use  $E_{hkl}$  in KeV and  $d$  in Angstroms. Fitting a given Bragg line allows the precision determination of its center of gravity (in energy) and thereby the calculation of the  $d_{hkl}$  lattice spacings. The strain variation from position to position in the sample is then determined from the shifts in Bragg peak energy:

$$\varepsilon_{ii} = - \left( \frac{\Delta d}{d_0} \right) = \left( \frac{\Delta E}{E} \right).$$

Here  $\Delta d = d - d_0$  is the change in the lattice spacing,  $d_0$  is the lattice spacing of the stress-free materials,  $\Delta E = E_0 - E$  is the correspondent peak shift and  $E_0$  is the center of gravity of peak of the stress-free material. The strain tensor  $\varepsilon$  can be determined by measuring strain in different directions in the samples and the stress tensor  $\sigma$  calculated using Hooke's law. In the analysis either the shifts in a single Bragg line, or in a statistical average of a collection of Bragg lines can

be used to calculate strain results. The difference in lattice parameter spacing between the two points achievable by this technique is ( $\Delta d \sim \pm 0.0001 \text{ \AA}$ ) [4-6].

Figure A3 shows the variation of the  $\epsilon_{33}$  and  $\epsilon_{11}$  strain components within 1mm of the peened surface this Ti-6Al-4V specimen, along with inset schematics of the gauge volume and sample geometry used in these measurements. It is important to note that the height of the incident x-ray beam (and spatial resolution) in the  $x_3$  direction in these measurements was  $20 \mu\text{m}$  similar to the resolution being used in the current program.

An EDXRD strain mapping study carried out by our group on a  $\sim 5 \text{ mm}$  thick Ti-6Al-4V shot peened specimen provides a good illustration of the techniques being used in this project. Specifically the very high spatial resolution strain measurements on a specimen with a biaxially

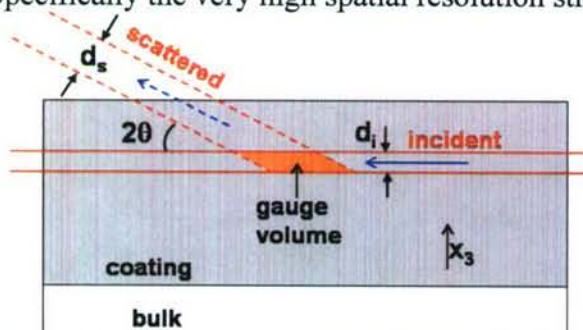


Figure A1. Schematic of the gauge volume, incident and diffracted beams used in the EDXRD measurements. Note that the  $x_3$  direction appropriate for the experiments in the main portion of the text is indicated

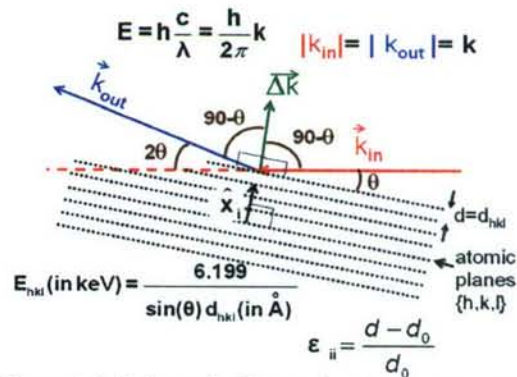


Figure A2. Schematic illustrating the small angle diffraction used in the EDXRD technique. Note that the inner atomic planes and their spacings are indicated.

surface stressed layer ( $\sim 200 \mu\text{m}$  plastically deformed shot peened layer) on an underlying thick substrate material.

The very different detailed-shaping of the diffraction (gauge) volumes in these two measurements are indicated schematically in the insets of Figure A3. For the  $\epsilon_{33}$  measurement the incident beam collimation  $d_i$  was  $20 \mu\text{m}$  along  $x_3$  (as noted above). In order to increase the diffraction signal, the scattered beam collimation,  $d_s$ , was increased to  $\sim 200 \mu\text{m}$ , greatly expanding the gauge volume along  $x_2$  (parallel to the surface). The collimation width along the  $x_1$  direction, parallel to the peened surface, was  $\sim 200 \mu\text{m}$ . For the  $\epsilon_{11}$  measurement, the sample was rotated by  $90^\circ$ ; the collimation perpendicular to  $x_3$  was  $30 \mu\text{m}$ ; and the incident  $d_i$  was expanded to  $\sim 100 \mu\text{m}$  (for increased signal), since it was now along the in-plane  $x_1$  direction; and  $d_s$  was increased to  $\sim 300 \mu\text{m}$ , also to increase the scattered signal.

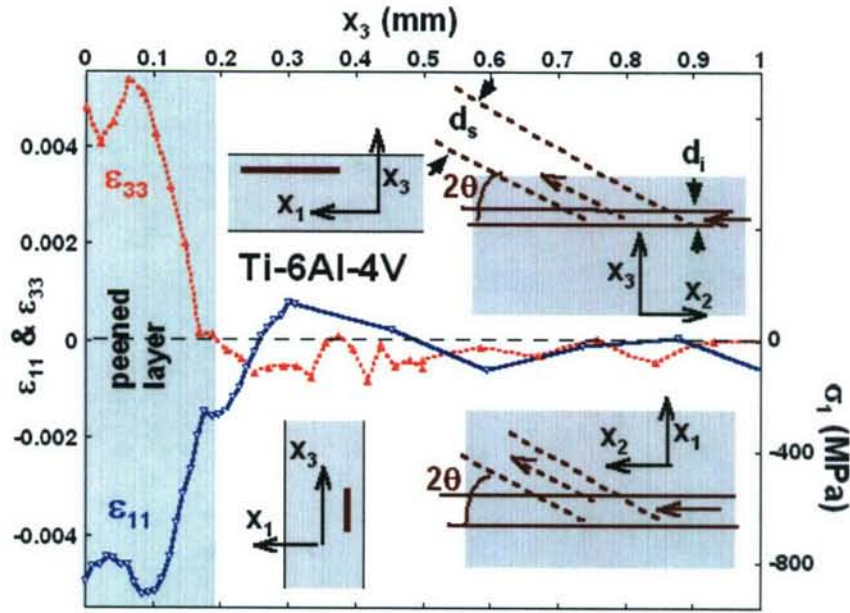


Figure A3. The strain profiles of  $\epsilon_{33}$  and  $\epsilon_{11}$  in the vicinity of the peened surface layer and the underlying bulk material of the Ti-6Al-4V specimen. The insets illustrate the x-ray scattering geometries for the  $\epsilon_{33}$  (top) and  $\epsilon_{11}$  (bottom) measurements. Note the stress scale (lower right) uses  $E=118$  GPa and  $\nu=0.33$  (see text) and  $\sigma_1=175 \epsilon_{11}$  [MPa].

The compressive in plane  $\epsilon_{11}$  strain and tensile  $\epsilon_{33}$  strain results in Figure A3 are in accord with the biaxial in-plane stress expected in the plastically deformed shot peened layer [12-15,7]. For biaxial symmetry,  $\epsilon_{11}=\epsilon_{22}$  and  $\sigma_1=\sigma_2$ , where  $\sigma_i$ , is the stress in the  $i$ 'th direction. In this case,

$$\sigma_1 = \left[ \frac{E}{(1+\nu)(1-2\nu)} \right] \{ \epsilon_{11} + \nu \epsilon_{33} \} \quad \text{and} \quad \sigma_3 = \left[ \frac{E2\nu}{(1+\nu)(1-2\nu)} \right] \epsilon_{33} \left\{ \frac{(1-\nu)}{2\nu} + \frac{\epsilon_{11}}{\epsilon_{33}} \right\}, \quad (1a\&b)$$

where  $\nu$  is Poisson's ratio and  $E$  is Young's modulus. For Ti-6Al-4V,  $\nu=0.33$  and one obtains

$$\sigma_3 = \left[ \frac{3E}{2} \right] \epsilon_{33} \left\{ 1 + \frac{\epsilon_{11}}{\epsilon_{33}} \right\}. \quad (2)$$

Since the experimental results in Figure A3 indicate that, to a very good approximation,  $\epsilon_{11} \sim -\epsilon_{33}$ , one has  $\sigma_3 \sim 0$ . This is not at all unexpected in view of the free surface in the  $x_3$  direction. Indeed, in general  $\sigma_3=0$  leads to

$$\frac{\epsilon_{11}}{\epsilon_{33}} = -\frac{1-\nu}{2\nu} \quad \text{and} \quad \sigma_1 = \epsilon_{11} \left[ \frac{E}{(1-\nu)} \right], \quad (3a\&b)$$

the former of which reduces to the observed  $\epsilon_{11} \sim -\epsilon_{33}$  for  $\nu=0.33$ . Further, using  $E=118$  GPa for Ti-6Al-4V, one obtains the in-plane stress scale  $\sigma_1=175 \epsilon_{11}$  [MPa], which is shown in the right and scale of Figure A3. It is important to note here that this stress calculation is an approximation, although a reasonable one, since it ignores the differences between the crystallographic-direction dependent elastic constants and bulk elastic properties [7].

## 7. References

- [1] Handbook of thermal spray technology, Eds J.R. Davis and Associates, ASM International, 2004.
- [2] Yourong Liu , Traugott E. Fischer, Andrew Dent, "Comparison of HVOF and plasma-sprayed alumina-titania coatings—microstructure, mechanical properties and abrasion behavior. " Surface and coatings technology, 167 (2003) 68–76.
- [3] E.H. Jordan, M. Gell, Y.H. Sohn, D. Goberman, L. Shaw, S. Jiang, M. Wang, T.D. Xiao, Y. Wang, P. Strutt, "Fabrication and evaluation of plasma sprayed nanostructured alumina–titania coatings with superior properties." Materials Science and Engineering A301 (2001) 80–89.
- [4] [7] M. Croft, I. Zakharchenko, Z. Zhong, Y. Gulak, J. Hastings, J. Hu, R. Holtz, M. DaSilva, and T. Tsakalacos, J. App. Phys. 92 ,578-586 (2002) and references therein
- [5] [8] M. Croft, Z. Zhong, N. Jisrawi,I. Zakharchenko, R.L. Holtz,Y. Gulak, J. Skaritka, T. Fast, K. Sadananda, M. Lakshmipathy, and T. Tsakalacos. Int. J. Fatigue 27, 1409 (2005) and ref. therein
- [6] [9] M. Croft, N. Jisrawi,Z. Zhong, R. Holtz, K. Sadananda, J. Skaritka, and T. Tsakalacos' to be published Int. J. Fatigue (2007)
- [7] G Brunoy and B D Dunnz Meas. Sci. Technol. 8 (1997) 1244–1249